CILAMCE 2017
Florianópolis - Santa Catarina - Brazil

Frequency-based Damage Detection Method above Work Frequency, Experimental Data

Horacio Valadares Duarte

Lázaro Valentim Donadon

hvduarte@ufmg.br

Depto. Engenharia Mecânica da Universidade Federal de Minas Gerais

Av. Antônio Carlos 6627, Zip-Code 31270-901, Pampulha, Belo Horizonte, M.G., Brasil

Abstract. *In this work the RSVD routine was used to identify damage in a structure using frequency response functions (FRFs) from a healthy and damaged aluminum plate with different failure levels. The RSVD was applied to FRFs in a high frequency range, above work frequency, as the main assumption is that small damages can be easily found by tracing the changes in high frequency modes. Though this assumption can be demonstrated theoretically, an actual measurement is usually difficult due to the environmental and measurement noise. This procedure can be an effective solution to those identification problems only if it proves to be practical and reliable. Some practical aspects will be discussed and actual data from different measurement positions, failure and noise level will be presented.*

Keywords: *Singular value decomposition, Structural health monitoring, Plate damage detection, Damage detection above work frequency.*

CILAMCE 2017
Proceedings of the XXXVIII Iberian Latin-American Congress on Computational Methods in Engineering
P.O. Faria, R.H. Lopez, L.F.F. Miguel, W.J.S. Gomes, M. Noronha (Editors), ABMEC, Florianpolis, SC, Brazil, November 5-8, 2017

INTRODUCTION

The use of modal analysis in Structural Health Monitoring, SHM, is a natural consequence of its use in structural dynamics. Changes in the dynamic response of the structure are linked to changes in stiffness, mass or damping of the structure and those make up the basic idea of Structural Health Monitoring (Shane and Jha, 2011). Many techniques are proposed to detect damages based on changes in modal parameters, a comprehensive review on modal parameters-based damage identification can be found in Fan (Fan and Qiao, 2011).

Difficulties that arise from different structural size and complexity, apparatus to excite the structure, material behaviour, environmental and loading changes have turned structural health monitoring into a challenging subject. Development in sensors and the increasing use of input from other areas are leading SHM towards an interdisciplinary approach.

There are some techniques that do not come directly from modal parameter procedures. A successful method is the ultrasonic guided waves, in particular Lamb waves (Lin, Giurgiutiu, and Kamal, 2012) in the frequency range from 15kHz to 800 kHz (Lin and Giurgiutiu, 2006), which are aimed at plate-like structures (Konstantinidis, Drinkwater, and Wilcox, 2006). Their ability to detect damages has been demonstrated by published results (Konstantinidis et al., 2006). The measurements are usually done in high frequency using piezoelectric sensors or piezoelectric wafer active sensors (PWAS). They can be brittle piezoceramic (PZT) wafers used on ultrasonic guided wave, or flexible piezoelastic polymers such as PVDF (Lin and Giurgiutiu, 2006). Being thin and light they can be bonded or embedded in the structure.

With the same installation of PWAS transducers, one can apply a variety of damage detection methods (Lin et al., 2012; Lin and Giurgiutiu, 2006). Another successful method, using PWAS, in a frequency range typically greater than 30 kHz (Park and Inman, 2007), was named piezoelectric Impedance Method . A brief overview can be found in the paper by Park and Inman (2007).

Methods based on modal parameters work with low frequencies, mainly with the first natural frequencies, that make it possible to obtain detailed mode shapes, basic data for almost all damage detection techniques (Fan and Qiao, 2011; Qiao, Lestari, Shah, and Wang, 2007). A well defined shape mode is easily obtained for low frequency modes, and some techniques use PWAS for direct shape measurements or scanning laser vibrometer Qiao et al. (2007).

The former methods using modal parameters were those using change in natural frequency. Relatively simple to measure they are cost effective (Kim and Stubbs, 2003). Kim and Stubbs (2003) present a crack location model and a crack size estimation model by relating fractional changes in modal energy to changes in natural frequencies. The method needs a Finite Element Model, FEM, of the structure.

The main problem in this kind of technique is the small change in frequencies also found for a big damage, Zhong (Zhong, Oyadiji, and Ding, 2008) relates a change of 5% for the first mode of bending vibration frequency when the crack ratio is greater than

50%. From Kim and Stubbs (2003) the modal strain energy can be computed as

$$W_i = \frac{1}{2}\int_0^L EI(\phi_i'')^2 dx \tag{1}$$

where W_i is the strain modal energy for ith mode shape, ϕ_i, and ϕ_i'' its curvature, EI is the beam stiffness, L its span length. So the strain energy depends on the squared curvature. Kim and Stubbs (2003) presented an equation associating ith eigenvalue change, $\delta\lambda_i$ ($\lambda_i = \omega_i^2$), to change in strain modal energy :

$$\frac{\delta\lambda_i}{\lambda_i} \approx \frac{\delta W_i}{W_i} \tag{2}$$

Those methods based on modal parameters are sensitive to changes in environment, operational conditions and structural uncertainties (Vanlanduit, Parloo, Cauberghe, Guillaume, and Verboven, 2005), sensor system, measurement quality (Zhong et al., 2008; Qiao et al., 2007) and noise (Fan and Qiao, 2011; Zhong et al., 2008).

The Proper Orthogonal Decomposition (POD) method has been proposed aiming to remove the influence of these external factors (Vanlanduit et al., 2005; Shane and Jha, 2011). The POD is a powerful multi-variate statistical method for data analysis aimed at obtaining low-order approximate descriptions of a high-dimensional process (Wu, Liang, Lin, Lee, and Lim, 2003). The POD is an orthogonal transformation that decorrelates the signal components and maximizes variance. This is the way that the POD method reduces a large number of interdependent variables to a smaller number of uncorrelated variables (Kerschen, Golival, Vakakis, and Bergman, 2005). The discrete implementation of the proper orthogonal decomposition is the popular Singular Value Decomposition Method, SVD (Kerschen and Golinval, 2002; Wu et al., 2003).

There are different implementations of the proper orthogonal decomposition method to structural health monitoring. Vanlanduit et al. (2005) proposed the robust singular value decomposition method (RSVD), which uses the frequency response functions (FRFs) of displacement, force, acceleration or other output as a basic data for the method. This technique can be considered a frequency method which uses the Singular Value Decomposition to remove external factors with statistics to find out damaged measurement sets.

This work is closely related to the implementation of the Robust Singular Value Decomposition method (RSVD) as published by Vanlanduit (Vanlanduit et al., 2005), which could find fault signals on a set with healthy and damaged data. The main assumption in High Frequency-based Damage Detection Method is that small damages can be more easily found by changes in high frequency modes. In other words assuming that they are more likely to present great FRF shape changes at high frequency.

These expected changes at high frequency can be explained by equation (1), which shows that the strain energy depends on the squared curvature, and that high modes present more curve changes and more accentuate curvatures so its strain energy is high. Using equation (2) Kim and Stubbs (2003) with a small change:

$$\frac{\delta\lambda_i}{\lambda_i} \approx \frac{\delta W_i}{W_i} \quad \rightarrow \quad \delta\lambda_i \approx \lambda_i\frac{\delta W_i}{W_i} \tag{3}$$

one can observe that small damages can be first observed in the high frequency range as the change in modal energy is multiplied by its frequency($\lambda_i = \omega_i^2$). So the main response of the structure is less affected by small damage.

This focus on high frequency allows to employ all modal analysis techniques and to gather more information about the problem at a further stage. For some applications it is also possible to get data far from work frequencies and their noise environment avoiding the need to stop the equipment to collect data to service it (Devriendt, Magalhaes, Weijtjens, Sitter, Cunha, and Guillaume, 2014). But, as stated, this procedure can be effective only if one can trust the measurement taken. So an actual measurement with different measurement position and noise level must be conducted following a statistical procedure.

Within this frequency range there is more measurement noise and sensor position change is sometimes critical for results. The feasibility of the method is related to a precise, reliable measurement. Thus traditional accelerometer sensors were replaced with fixed PZT sensors allowing for good repeatability of measurements, essential in this frequency range. This fixed PZT can be shared with other techniques as one of them should not exclude the other.

The dataset used in this work were measured using FRF data from a metallic Aluminium plate in which a mass was attached to it to simulate a damage. The sensitivity analysis of the detection algorithm was performed using a set of FRFs from damaged and healthy structure. The measurements were taken at the same PZT, for both healthy and damaged structure, and the excitation PZT was also at the same position.

Unlike previous reported cases, frequency ranges from 2 kHz to 12 kHz, the detection algorithm was tested for a frequency ranges from 1.3 kHz to 2.3 kHz. In this text the expression 'high frequency' will be used for those frequencies were wave-length of the structural mode shape is very small relative to length or width of the structure.

For this frequency range the FRFs were taken from different measurement positions and two damaged level.

Damage Detection Algorithm

The classical Least-Squares SVD-based damage detection can be outlined as follows. The database is obtained from Frequency Response Function (FRF), a $P \times N$ matrix $H = [H_1, H_2, ...H_N]$ at N specified conditions, in which each column H_n is a FRF data of dimension P. $N = N_u + N_d$ where N_u represents the undamaged experimental FRFs from healthy structure and N_d is from damaged ones. The damaged database $N_D = \sum N_d$ must be equal or greater than $N_U = \sum N_u$. The sequence steps of the damage detection algorithm are presented below.

1- Computing the SVD of the $P \times N$ matrix $H = USV^H$;
2- Taking only significant singular values from $S = diag(s_1, s_2, .., s_N)$, above the noise level $S1 = diag(s_1, s_2, .., s_k, 0, 0, .., 0)$;
3- Using the singular vectors U and V from original matrix to synthesize a matrix $H1$ of rank k, such as $H1 = US1V^H$;
4- Computing a residual matrix $E1$, $E1 = H - H1$;
5- Performing the variance s of the residuals:

$$s = \frac{1}{MN-1}\sum_{i=1}^{M}\sum_{j=1}^{N}(H_{i,j} - H1_{i,j})^2 \tag{4}$$

6- Computing the variance of each measurement j (each column j from matrix H and from $H1$):

$$s_j = \frac{1}{M-1}\sum_{i=1}^{M}(H_{i,j} - H1_{i,j})^2 \tag{5}$$

7- Estimating the relative distance d_j^{SVD} of each measurement j to subspace computed by SVD:

$$d_j^{SVD} = \frac{s_j}{s} \tag{6}$$

As the relative distance d_j^{SVD} is defined as a variance ratio it obeys a χ^2 distributionVanlanduit et al. (2005). For a χ^2 distribution with a confidence level of $(100-\alpha) = 95\%$ and for $(N_n - 1)$ degrees of freedom up to 30, $(N_n - 1) < 30$Vanlanduit et al. (2005), a threshold T can be defined as

$$T = \sqrt{\frac{\chi^2_{(100-\alpha)_{(N_n-1)}}}{2}} \tag{7}$$

If $d_j^{SVD} >$ threshold T, then there is a damaged sample. For N >30 a maximal value of T for N= 30 is taken in order to make sure that the threshold is not too tightVanlanduit et al. (2005).

The Robust SVD

The problem with the Least-Squares SVD based damage detection is that it is very sensitive to outliers in measurement. According to Vanlanduit et al. (2005), this problem can be overcome using Robust Singular Value Decomposition Method, RSVD. The RSVD does not compute the whole database H, it is computed only over $N/2$ observations, the original matrix is re-synthesized and the distances and errors are computed. The solution is the small cost function from all possible combinations of the database. The steps of the RSVD routine are given by,

1- Construct a matrix H_R from matrix H with $L = N/2$ combination columns from N columns of the original matrix.

a- computing the SVD of the matrix $H_R = U_R S_R V_R^H$;

b- computing the extended right singular vector $V_E = U_R^H S_R^{-1} H$;

c- computing re-synthesized matrix H_S using $H_S = U_R S_E V_E^H$, $S_E(i,i) = S_R(i,i)$ $i = 1, 2, ..., L$ and $S_E(i,i) = 0$ if $i > L$;

d- Computing the residuals $E_S = H - H_S$;

e- Computing the variance s of the residuals using the median absolute deviation MAD, modifying step 4 of SVD-based damage detection, $s = MAD(E_S)$, where:

$$MAD(E_S) = 1.4826 * median(|E_S - median(E_S)|) \tag{8}$$

f- Computing the variance for each measurement j (each column j):

$$s_j = \frac{1}{M-1} \sum_{i=1}^{L} (H_{i,j} - H_{S(i,j)})^2 \tag{9}$$

g- Estimating the relative distance d_j^{SVD} for each measurement j to the subspace computed by SVD:

$$d_j^{SVD} = \frac{s_j}{s} \tag{10}$$

h- computing the cost function $\kappa = \sum_j^L |d_j|^2$;
2- The minimal cost function κ is taken as the RSVD solution, $H_B = H_S$. The variance s and d_j^{SVD} are computed following the procedures from **d** to **g** in the previous steps. For a χ^2 distribution, the threshold T is the same as defined in Eq. 7 and the same confidence interval was employed.

EXPERIMENTAL SETUP

The experimental procedure was performed using dynamic response of a free Aluminium plate suspended by a thin nylon wire. The Aluminium plate is 1 m $\times$ 1 m, Fig.1. The measurement database was obtained from FRF response at measurement points A, B and D, Fig. 1, the reference was PZT 1 and excitation at PZT E, on plate opposite side just behind PZT 1 position, Fig. 1.

Using the excitation signal from PZT E as reference to obtain the FRFs at PZTs A, B and D has resulted in noisy FRFs at the intended frequency range. To improve the results, the reference signal was chosen to be from PZT 1, and not from the excitation signal PZT E. This procedure ensured a good signal to noise relation and improved the results.

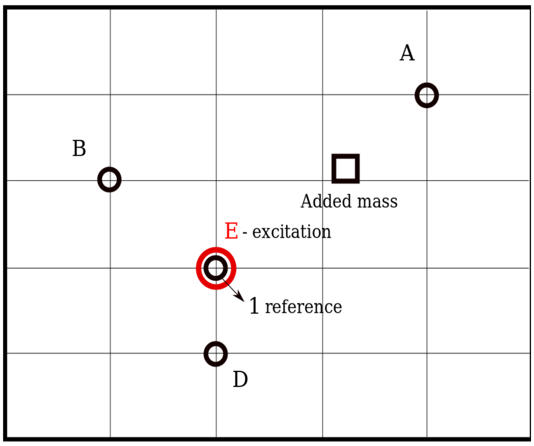

Figure 1: Aluminium plate and PZT sensor position.

Experimental data acquisition was performed by the PHOTON II from LDS. Measurements were done using two different excitation signals, white noise and sweep-sine signals both generated by the PHOTON II. From the generator the signal was send to amplifier and then to PZT E, Fig.2. All FRFs have units Volts/Volts (response/excitation)

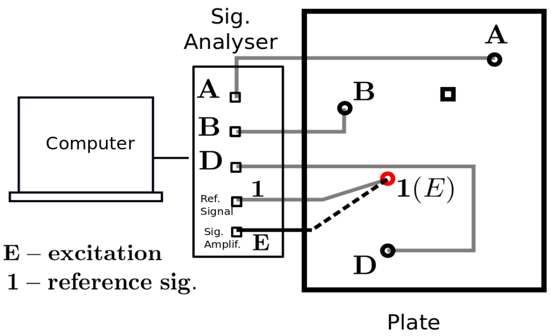

Figure 2: Measurement setup layout. PZT E (excitation), PZT 1 (signal reference), PZT A, B and D measurement.

in spam of 2.4 kHz and 3200 line resolution. The employed frequency, in the range from 1.3 to 2.3 kHz, was obtained using a Shaped Excitation Curve for random excitation signal, the same initial and final frequency defines the Swept Sine signal excitation range employed. Both Shaped Excitation Curve and Swept Sine are signal excitation functions implemented in data acquisition equipment.

The healthy structure has $1\,\mathrm{m}\times 1\,\mathrm{m}\times 1.0\times 10^{-3}\,\mathrm{m}$ and 2.7 kg, data from vendor, and the damaged structure had an added mass with 4.2×10^{-3} kg, and 9.7×10^{-3} kg for the second failure level case, which represents about 0.16% and 0.34% of the structure's mass respectively.

The measurement PZT diameter is $D_{PZT} \approx 6.5\,\mathrm{mm}$, with an area of $3.318\times 10^{-5}\mathrm{m}^2$. The passive or measurement PZT sensors 1, A, B and D are from Acellent Technologies. The diameter of excitation diaphragm PZT, PZT E, is $D^E_{PZT} \approx 18\,\mathrm{mm}$, placed behind reference sensor PZT 1, and its area is $2.5\times 10^{-4}\mathrm{m}^2$, approximately 0.03% of the plate area. Both added mass were placed at same position, squared mark at Fig. 1 and Fig. 2.

RESULTS AND ANALYSIS

The analysis presented in following sections were made using FRF data from PZT at positions A, B and D using PZT 1 as reference, Fig. 1 and Fig. 2. At each position there are 16 FRFs for healthy structure, the reference set was compounded by a subset with 8 FRFs using shaped random signal and 8 measurements using swept sine signal. The damaged set for 4.2×10^{-3} kg and and 9.7×10^{-3} kg added mass structure sets were made up in similar way. The RSVD results presented in this section has made use of shaped random signal only. The swept sine signal will be stated when used.

On Fig. 3 FRF from shaped random signal for healthy and 4.2×10^{-3} kg added mass from A position.

Results from PZT at Position A

On Fig. 4 there are the RSVD relative distance, d^{SVD}, graphic mark height, for each measurement, numbers on abscissa, threshold blue horizontal line. The first 8 measurements, on abscissa, are related to healthy reference set, and the following 8 marks to

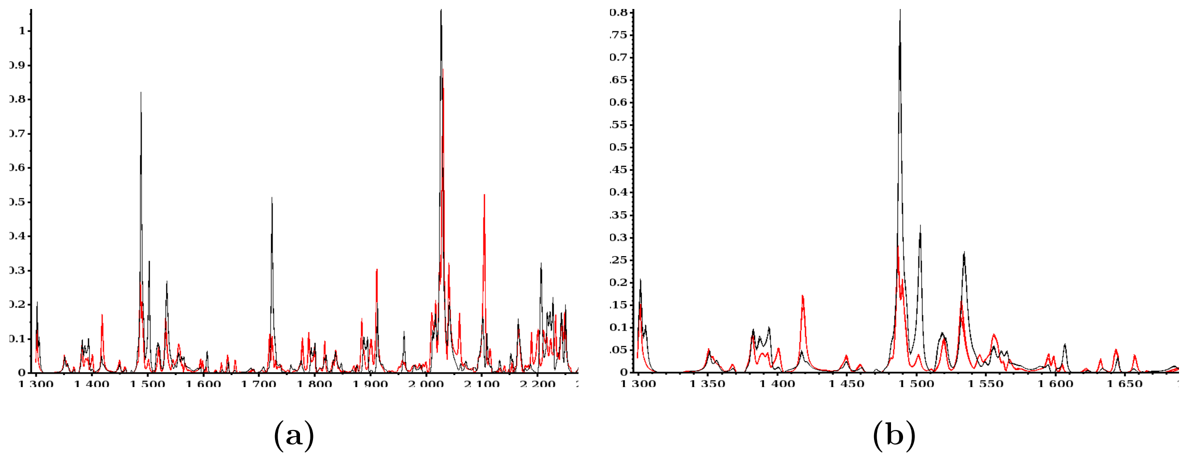

Figure 3: (a) FRFs from Position A. Healthy set with 8 measurements, black lines, red lines 4.2$\times 10^{-3}$ kg added mass. (b) FRF detail from 1.3 to 1.7 kHz.

damaged set, on the Fig.4-(a) there are the results for 4.2$\times 10^{-3}$ kg added mass structure. On Fig.4-(b) there are the results for 9.7$\times 10^{-3}$ kg added mass damaged structure. On Fig.4-(c) there are the RSVD result using signal from 4.2$\times 10^{-3}$ kg added mass and those from 9.7$\times 10^{-3}$ kg added mass damaged structure.

On Fig.4-(a), Fig.4-(b) and Fig.4-(c) there are two marks showing relative distance above the threshold line or damage. The results presented seems not be sensitive to mass difference of 4.2$\times 10^{-3}$ kg, 9.7$\times 10^{-3}$ kg and 4.5$\times 10^{-3}$ kg.

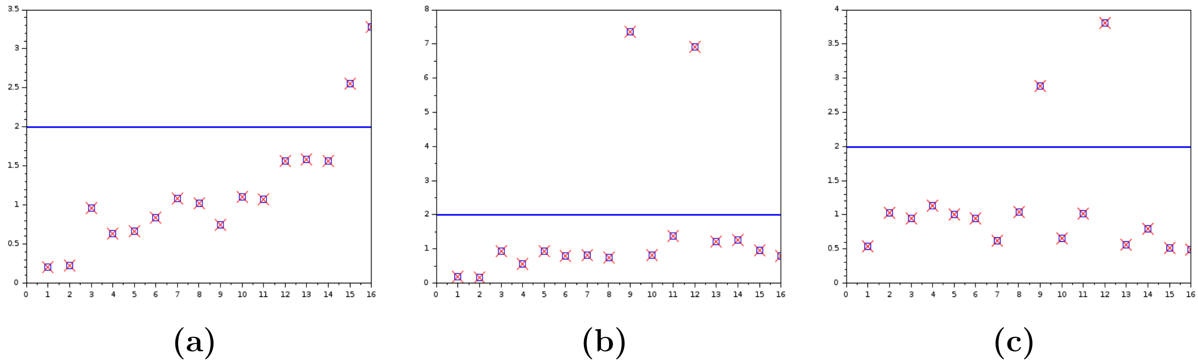

Figure 4: RSVD relative distances, d^{SVD}, on vertical axis, threshold blue horizontal line. (a) Results for reference and 4.2$\times 10^{-3}$ kg mass added structure, (b) reference signal and 9.7$\times 10^{-3}$ kg added mass dataset, (c) between 4.2$\times 10^{-3}$ kg and and 9.7$\times 10^{-3}$ kg added mass.

Results from PZT at Position B

On Fig.5-(a) and Fig.5-(b) one can see the results for 4.2$\times 10^{-3}$ kg and for 9.7$\times 10^{-3}$ kg added mass, on Fig.5-(c) RSVD the results for 4.2$\times 10^{-3}$ kg used as reference and the signal from 9.7$\times 10^{-3}$ kg added mass structure. As in the previous case the first 8 measurements, on abscissa, are related to healthy reference set, and the following 8 marks to damaged set.

On Fig.5-(a) and Fig.5-(b) there are only one mark showing relative distance above the threshold line or damage. On Fig.5-(c) comparing data between 4.2$\times 10^{-3}$ kg and

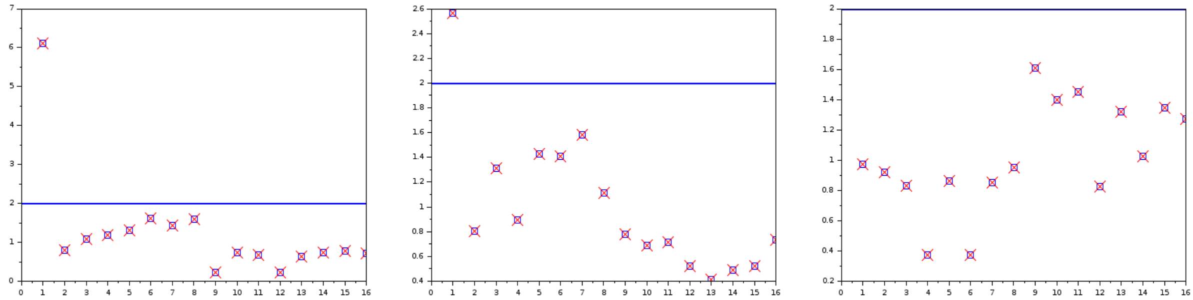

(a) (b) (c)

Figure 5: RSVD relative distances Position B, d^{SVD}, on vertical axis, threshold blue horizontal line. (a) Results for reference and 4.2$\times 10^{-3}$ kg mass added structure, (b) reference signal and 9.7$\times 10^{-3}$ kg added mass dataset, (c) between 4.2$\times 10^{-3}$ kg and and 9.7$\times 10^{-3}$ kg added mass.

9.7$\times 10^{-3}$ kg added mass there is no indication for relative distance, d^{SVD}, above threshold damage level.

On Fig.5-(a) and Fig.5-(b) the mark showing the damage was on healthy set in both cases and this is the outstanding aspect of those results. Those results deserve some comments as all failure indications, $d_j^{SVD} > T$, should be considered even occurring between healthy measurement sets. The failure indication is expected to show up on damaged measurement sets but knowing a healthy dataset in advance all distance above the acceptable level was considered a failure indication.

The algorithm deals only with relative distances, d_j^{SVD}, between datasets and there is no mathematics basis to believe that the healthy set would be the reference. A failure indication could appear in a healthy subset if there is a great data dispersion on that set.

Results from PZT at Position D

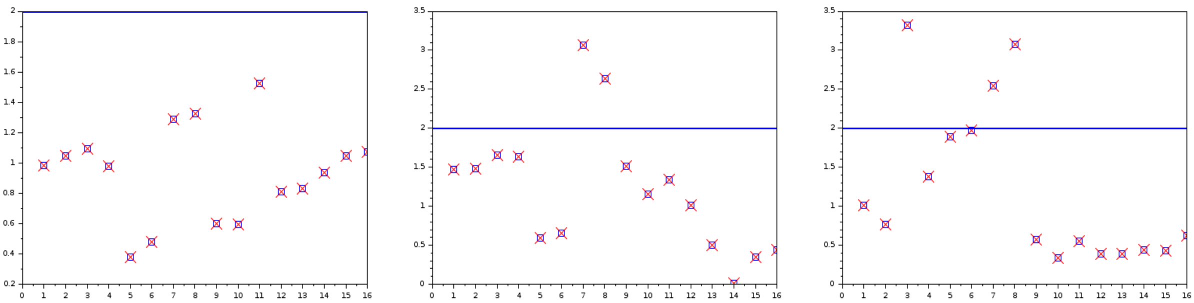

(a) (b) (c)

Figure 6: RSVD relative distances at Position D, d^{SVD}, on vertical axis, threshold blue horizontal line. (a) Results for reference and 4.2$\times 10^{-3}$ kg mass added structure, (b) reference signal and 9.7$\times 10^{-3}$ kg added mass dataset, (c) between 4.2$\times 10^{-3}$ kg and and 9.7$\times 10^{-3}$ kg added mass.

As in the previous cases, the first 8 measurements, on abscissa, are related to healthy reference set, and the following 8 marks to damaged set, on the Fig. 5-(a) there are no failure indication for 4.2×10^{-3} kg added mass structure. On Fig. 6-(b) there are two marks showing relative distance above the threshold line or damage on set for 9.7×10^{-3} kg added mass structure.

On Fig.5-(c) comparing data between 4.2×10^{-3} kg and 9.7×10^{-3} kg added mass there are tree indications for relative distance, d^{SVD}, above threshold damage level. This result a mass difference of 4.5×10^{-3} kg with better failure indications than for 9.7×10^{-3} kg suggest that the signal quality could be more significant. This statement is reinforced if comparing those results with those of Position B, that is closest to the damage site.

Again failure indication has appeared in a healthy subset.

False Positive

In this section will be presented the results between two sets, one from shaped random noise signal and other set from a swept-sine signal, both from same structure condition. This procedure has been used to assess the result quality for all positions and damaged levels so it was not only employed on healthy structure. The positive failure indication between signals from the same structure condition are named False Positives. Those results are only from Position A, there are no false positive case for Position B and D. The Position A is closest from added mass site, the FRFs response level has good level but the signal were more noisily as coherence was not so good as from other Positions. This is probably because the Position A has the farthest distance from reference Position 1 and the excitation point E.

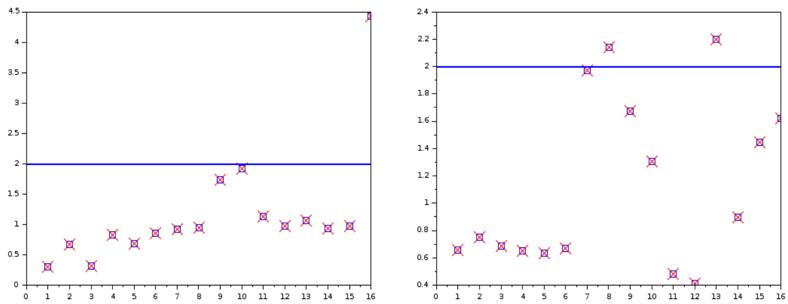

(a) (b)

Figure 7: False Positive RSVD results for shaped random $\times$ swept sine signals from the same structure condition. (a) for healthy structure , (b) for 4.2×10^{-3} kg added mass.

On Fig. 7-(a) there are the result between healthy structure set there is a failure indication for latest measurement. For 4.2×10^{-3} kg added mass damaged structure, Fig. 7-(b) there are two failure indications one for shaped random signal and one for swept-sine. There are no false positive for 9.7×10^{-3} kg added mass.

False Positive for different frequency ranges

Trying to get more information to improve knowledge on the problem the RSVD procedure was applied over 200 Hz frequency range from 1.3 to 2.3 kHz for both analysis where the false positive has taken place, healthy structure random and swept sine set and for 4.2×10^{-3} kg added mass. On Fig. 8 and Fig. 9 one can see the results for frequency range from 1.3 to 1.5 kHz, top left graphic, and from 1.5 to 1.7 kHz, top right graphic. The FRFs for the range from 1.3 to 1.7 kHz are on the bottom.

Those results are representative for whole range frequency groups. On top left graphic of Fig. 8 there are 3 false failure indications for frequency range from 1.3 to 1.5 kHz and, for this graphical resolution, one could scarcely found out differences between the 8 FRFs from shaped random signal, black lines, and swept-sine signal, red lines. On the other hand for 1.5 to 1.7 kHz, top right graphic, there is only one fault indication and it is observable differences between the measurements, resonant peak level and resonant frequency peaks changes, Fig. 8 bottom.

On top left graphic of Fig. 9 there is no false failure indications for frequency range from 1.3 to 1.5 kHz and one could found out remarkable differences between the 8 FRFs from shaped random signal, black lines, and swept-sine signal, red lines. In swept-sine signal there are a remarkable dispersion on results but it seems that the 'mean value' is similar to random noise signal. On the other hand for 1.5 to 1.7 kHz, top right graphic, there are two fault indications and it is observable differences between the measurements 'mean value', Fig. 9 bottom.

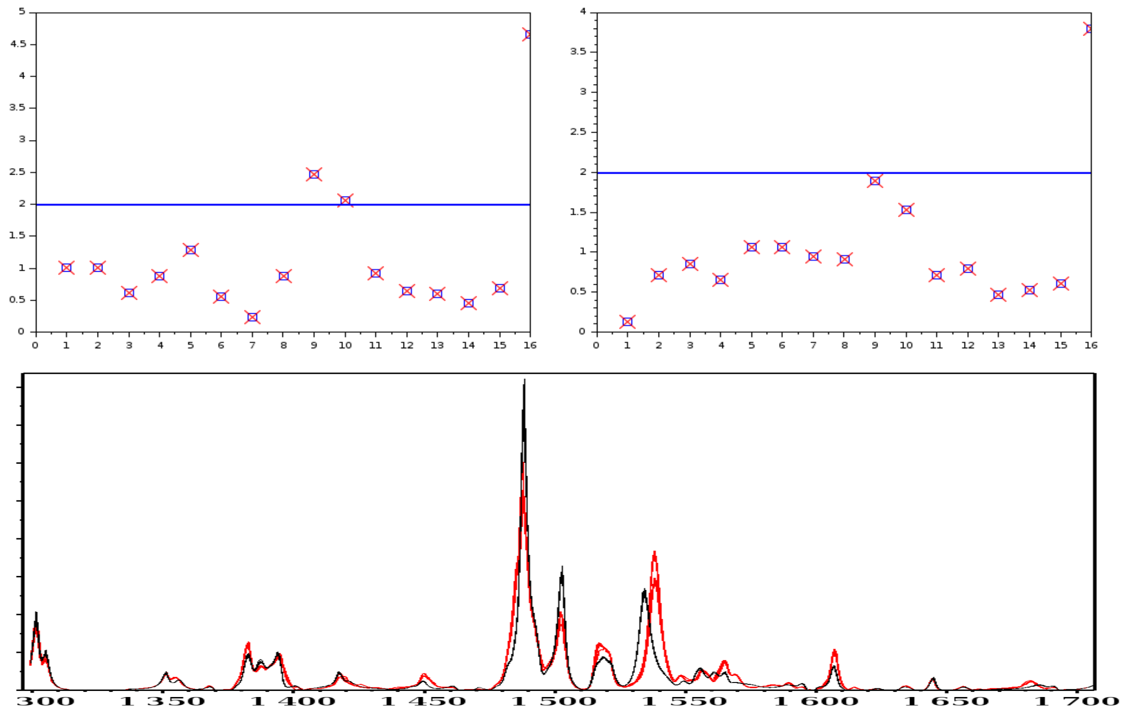

Figure 8: False Positive for shaped random and swept sine signal from healthy structure. Top left, FRFs from 1.3 to 1.5 kHz, top right, FRFs from 1.5 to 1.7 kHz. Bottom, FRFs for shaped random, black lines, and swept sine red lines from 1.3 to 1.7 kHz.

For comparison on Fig.10, there are the RSVD results, for random noise signal, between healthy reference set, and the damaged 4.2×10^{-3} kg added mass structure set, for frequency ranges from 1.3 to 1.5 kHz and for 1.5 to 1.7 kHz . RSVD results for frequency range from 1.3 to 2.3 kHz results for this set and for same signal was presented on the Fig. 4-(a).

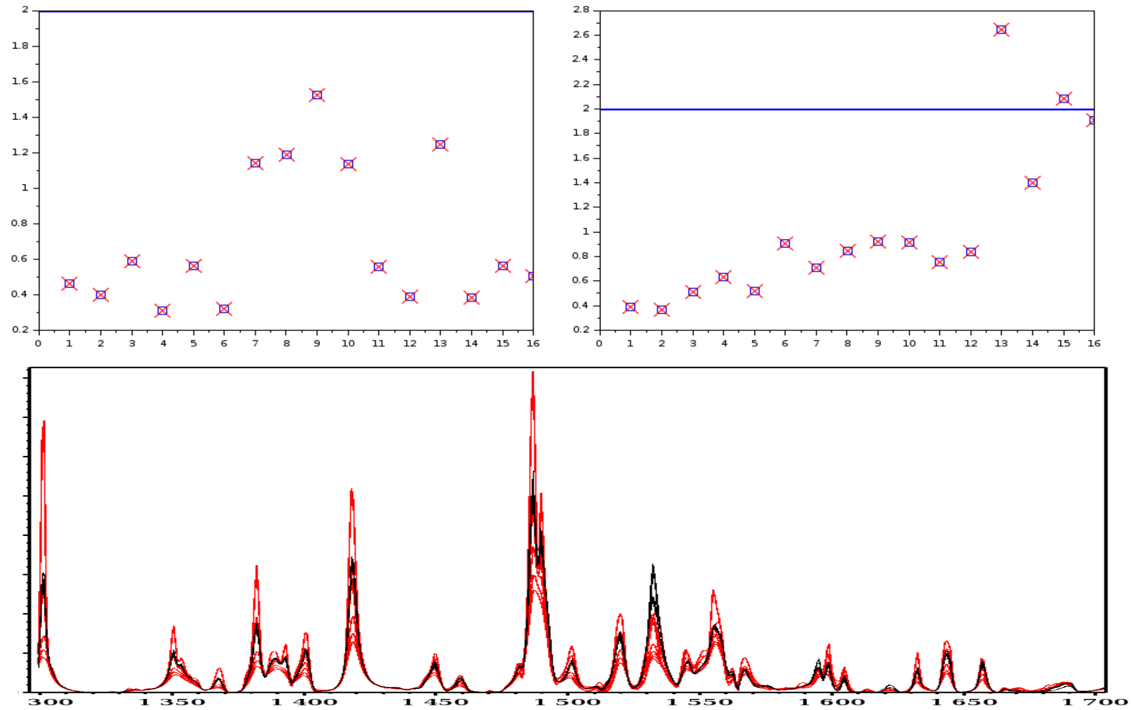

Figure 9: False Positive for shaped random and swept sine signal from 4.2×10^{-3} kg added mass structure. Top left, FRFs from 1.3 to 1.5 kHz, top right, FRFs from 1.5 to 1.7 kHz. Bottom, FRFs for shaped random, black lines, and swept sine red lines from 1.3 to 1.7 kHz.

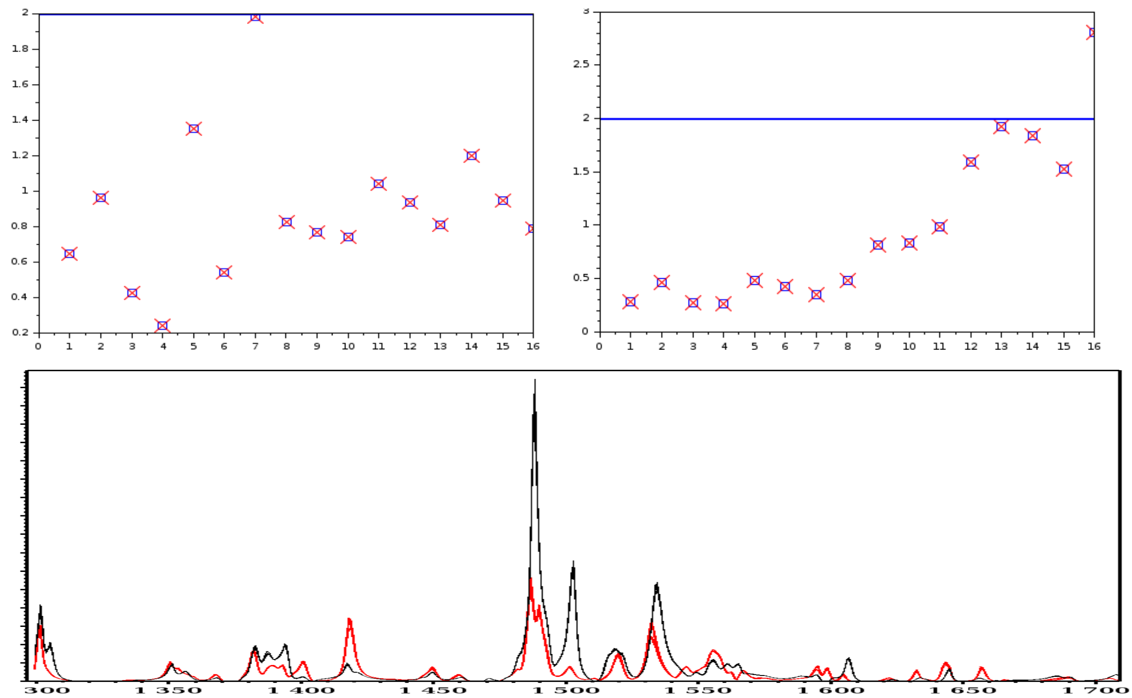

Figure 10: False Positive for healthy structure shaped random × swept sine, first column, for 4.2×10^{-3} kg added mass shaped random × swept sine, second column, last column the positive falure indication for healthy × 4.2×10^{-3} kg added mass range both for shaped random signal.

Those graphics present a interesting behaviour, there is a outstanding difference between the healthy structure, black lines, and the FRFs 4.2×10^{-3} kg added mass structure, red lines. But this difference are poorly present on failure results. This subject has comprehensive treatment on incoming paper Singular Value Noise In RSVD Algorithm for Damage Detection, (Duarte and Donadon, 2017).

CLOSING REMARKS

First some aspects related to position and distance from the reference, measurement point and failure place should receive some comments. The measurement position and its distance to failure position does not appear to impair the failure indication. Some aspects must be highlighted, the signal level from Position D, the further position from added mass position and closest to reference signal has been showed the lowest FRF signal level and a low noise signal. This Position D presented better results than those from Position B with similar distances.

Position A is the nearest from the failure position and furthest from the Reference Position 1 and it has displayed the highest signal level and the FRFs has been at least one magnitude order above the Positions B and D, Fig.1. However the signal from Position A presented a worst coherence when compared to other positions, in other words there are more noise on FRF signal. This, of course is related to the distance from the Excitation, in this setup, at the same position of the Reference Point. So lowest distance from the Excitation seems to be more effective than the distance from the failure site.

In swept-sine signal the swept period was not controlled and that could improve the noise in measurement. This noisily signal could not explain the changes between random noise and swept-sine FRF for same structure condition at Position A, as it were observed on Fig.8 and Fig.9. This false positive is treated in other paper and is related to correct choice of optimal singular value basis above the noise,(Duarte and Donadon, 2017).

Other aspect is the significant change in FRFs from healthy and damaged structure. The expectation was identification for frequencies that could be obtained by usual Modal Analysis equipment, but this change in FRFs was not expected, mainly because the PZT low level excitation energy. The structure is slender with low stiffness and in some measurements presented nonlinear response that was cut out. For this frequency range the fault identification at about 0.16% and 0.34% of the structure total mass it should partially related to structure lack of stiffness. Although the lack of stiffness could helped the identification in the frequency range, the main objective was reached that is a fault identification below 0.5% of the structure mass. It is the most important result as it could be considered a initial damage.

REFERENCES

C. Devriendt, F. Magalhaes, W. Weijtjens, G. D. Sitter, A. Cunha, and P. Guillaume. Structural health monitoring of offshore wind turbines using automated operational modal analysis. *Structural Health Monitoring*, 13(6):644–659, 2014. doi: 10.1016/j.jsv.2016.08.024.

H. V. Duarte and L. V. Donadon. Singular value noise in rsvd algorithm for damage detection. In *P.O. Faria, R.H. Lopez, L.F.F. Miguel, W.J.S. Gomes, M. Noronha eds, Proceedings of the XXXVIII Iberian Latin-American Congress on Computational Methods in Engineering ABMEC*, pages 1–14, Florianpolis, Brazil, 2017.

W. Fan and P. Qiao. Vibration-based damage identification methods: A review and comparative study. *Structural Health Monitoring*, 10(1):83–111, 2011. doi: 10.1177/1475921710365419.

G. Kerschen and J. C. Golinval. Physical interpretation of the proper orthogonal modes using the singular value decomposition. *Journal of Sound and Vibration*, 249(5)(5):849–865, 2002. doi: 10.1006/jsvi.2001.3930.

G. Kerschen, J. Golival, A. F. Vakakis, and L. A. Bergman. The method of proper orthogonal decomposition for dynamical characterization and order reduction of mechanical systems: an overview. *Nonlinear Dynamics*, 41:147–169, 2005.

J.-T. Kim and N. Stubbs. Crack detection in beam type structure using frequency data. *Journal of Sound and Vibration*, 259(1):145–160, 2003. doi: 10.1006/jsvi.2002.5132.

G. Konstantinidis, B. W. Drinkwater, and P. D. Wilcox. The temperature stability of guided wave structural health monitoring systems. *Smart Materials and Structures*, 15 (4):967, 2006. URL `http://stacks.iop.org/0964-1726/15/i=4/a=010`.

B. Lin and V. Giurgiutiu. Dynamics-based damage detection of composite laminated beams using contact and noncontact measurement systems. *Smart Materials and Structures*, 15:1085–1093, 2006. doi: 10.1088/0964-1726/15/4/022.

B. Lin, V. Giurgiutiu, and A. M. Kamal. The use of exact lamb waves modes for modeling the power and energy transduction of structurally-bonded piezoelectric wafer active sensors. In *Proceedings of SPIE Smart Structure and Materials, Nondestructive Evaluation and Health Monitoring, Sensors and Smart Structures Technologies for Civil, Mechanical, and Aerospace Systems 11-15 March, 2012*, pages 1–12, San Diego, CA, 11-15 March 2012. URL `http://www.me.sc.edu/research/lamss/pdfnew/Conferences/-C199_SS12-8345-8_7Mar2012_BL.pdf`.

G. Park and D. J. Inman. Structural health monitoring using piezoelectric impedance measurements. *Philosophical Transactions of The Royal Society A*, 365:373–392, 2007. doi: 10.1098/rsta.2006.1934.

P. Qiao, W. Lestari, M. G. Shah, and J. Wang. Dynamics-based damage detection of composite laminated beams using contact and noncontact measurement systems. *Journal of Composite Materials*, 41:1217–1252, May 2007. doi: 10.1177/0021998306067306.

C. Shane and R. Jha. Proper orthogonal decomposition based algorithm for detecting damage location and severity in composite beams. *Mechanical Systems and Signal Processing*, 25:1062–1072, 2011. doi: 10.1016/j.ymssp.2010.08.015.

S. Vanlanduit, E. Parloo, B. Cauberghe, P. Guillaume, and P. Verboven. A robust singular value decomposition for damage detection under changing operating condtions and structural uncertainties. *Journal of Sound and Vibration*, 284:1033–1050, 2005. doi: 10.1016/j.jsv.2004.07.016.

C. Wu, Y. Liang, W. Lin, H. Lee, and S. Lim. Letter to the editor: A note on equivalence of proper orthogonal decomposition methods. *Journal of Sound and Vibration*, 265:1103–1110, 2003. doi: 10.1016/S0022-460X(03)00032-4.

S. Zhong, S. O. Oyadiji, and K. Ding. Response-only method for damage detection of beam-like structures using high accuracy frequencies with auxiliary mass spatial probing. *Journal of Sound and Vibration*, 311:1075 – 1099, 2008. doi: 10.1016/j.jsv.2007.10.004.